Letter

Statistical dependencies beyond linear correlations in light scattered by disordered media

Ilya Starshynov,* Alex Turpin, Philip Binner, and Daniele Faccio†
School of Physics & Astronomy, University of Glasgow, Glasgow G12 8QQ, United Kingdom

(Received 12 November 2020; revised 19 September 2021; accepted 30 March 2022; published 11 May 2022)

Imaging through scattering and random media is an outstanding problem that, to date, has been tackled by either measuring the medium transmission matrix or exploiting linear correlations in the transmitted speckle patterns. However, transmission matrix techniques require interferometric stability and linear correlations, such as the memory effect, can be exploited only in thin scattering media. Here we show the existence of a statistical dependency in strongly scattered optical fields in a case where first-order correlations are not expected. We also show that this statistical dependence and the related information transport is directly linked to artificial neural network imaging in strongly scattering, dynamic media. These nontrivial dependencies provide a key to imaging through dynamic and thick scattering media with applications for deep-tissue imaging or imaging through smoke or fog.

DOI: 10.1103/PhysRevResearch.4.L022033

I. INTRODUCTION

The statistics of individual speckle patterns created by coherent illumination of an optically random medium is well understood. It is widely accepted that, as the real and imaginary parts of the scattered field are uncorrelated Gaussian random variables, the field amplitude follows a Rayleigh distribution and the light intensity follows a negative exponential distribution [1]. Identifying the correlation statistics of scattered light is a more challenging problem. Various types of correlations in space, time, or frequency may exist in the scattered fields, depending on the problem geometry and disorder strength [2,3]. A particularly relevant configuration involves imaging through a scattering slab, where a common goal is to reconstruct the image of an object from the transmitted scattered light. The strongest and most evident of the field correlations, the memory effect (ME) [3,4], has proven to be useful in such a situation, for example, allowing to reconstruct the image from a simple autocorrelation calculation of the speckle pattern [5–7]. Recently, more subtle, long-range mesoscopic correlations emerging in strongly scattering media [8] have been used to retrieve the image of a hidden object [9]. However, first-order correlations capture only a fraction of the total statistical dependence between random variables [10].

The dependence between random variables can be embedded into higher-order correlations even when the first-order correlation is zero. As quantifying all the higher-order correlations can be challenging especially for the case of multiple variables, usually information-theoretical criteria are applied to analyze a statistical dependence. In particular, nonzero mutual information (MI) implies a dependence between the random variables. Information theory approach has been applied to wave scattering in the context of radio-wave communication [11], albeit focusing more on temporal or frequency modulations rather than spatial information [12–14]. In recent work [15], the universal bounds of spatial information preserved in multiple scattering were estimated within the context of random matrix theory [16], thus neglecting the details of a realistic optical random scattering potential.

Alternatively to a stochastic approach to the characterisation of multiple scattering media, it is possible to formulate a deterministic description based on a transmission matrix (TM) measurement [17,18]. This complex-valued matrix completely characterizes the mapping between the input and output fields and, once known, can be used to calculate the input field distribution from the output speckle pattern. The TM approach has been successfully applied to both diffuse imaging and imaging through multimode fibers [19,20]. However, it suffers from the main drawback that it is sensitive to optical wavelength scale changes in the scattering medium. Measuring the transmission matrix typically requires some form of holography that needs to be repeated for a number of input modes and therefore is very challenging to extend to dynamic scattering media such as live tissue or fog. Even apparently static media such as white paint are known to evolve over relatively short timescales [21].

The TMs of typical disordered media can also be extremely large, so data-driven approaches seem a reasonable way to tackle the resulting complicated mapping between the input and output patterns. Machine learning and artificial neural networks (ANNs) have therefore been increasingly applied over the past few years to the problem of classifying objects or imaging through scattering media [22–26]. These methods, however, tend to suffer from the same drawback as

*ilya.starshynov@glasgow.ac.uk
†daniele.faccio@glasgow.ac.uk

the TM approaches, i.e., minimal changes of the scattering medium deteriorate or render the reconstruction impossible. Recently, a convolutional neural network based on the U-net architecture [27] was shown to be capable of reconstructing the image of a hidden object through optical disorder, while being trained on similar, but different disorder realizations [28]. These results were demonstrated in a very thin diffuser that will therefore exhibit a marked (i.e., wide-angle) ME. A recent extension to the case of multimode fibers was explained as the result of weak but nonzero correlations [29].

In this work we demonstrate the presence of a statistical dependence in the optical field distribution transmitted through a random medium. We purposely consider a system in which no memory effect or any other linear correlations could be present, which is achieved by stacking two glass diffusers at a distance from each other. Numerical modeling allows us to calculate the amount of MI between discretized input and output fields, which gives us an estimate of the input image information carried through this scattering system. We then verify the ability of a U-Net ANN to also image handwritten digits and show that the image reconstruction quality depends on the amount of mutual information. Remarkably, we also find a similar quality image reconstruction in the presence or absence of the memory effect that underlines the unexpected dominant role played by these statistical dependencies in supervised imaging approaches. These findings extend the current paradigms for diffuse imaging to random media that are both dynamic and strongly scattering and provide a key to imaging in various scenarios ranging from dynamic multimode fiber endoscopes to imaging through fog and tissue.

II. RANDOM SCATTERING BEYOND THE MEMORY EFFECT

The scattering configuration we consider is typical to a number of imaging through obscuration experiments, see Fig. 1(a). A collimated laser beam illuminates a spatial light modulator (SLM). The SLM is imaged by a $4f$ lens system onto a camera. The random scattering medium is made of one or two ground glass diffusers (220 grit, Thorlabs) separated by 5 mm and positioned between the SLM and the first lens of the imaging system.

One of the main goals of this work is to investigate the underlying physics of imaging through unknown or dynamic scattering media in the absence of the ME, i.e., in a regime in which standard approaches based on the measurement of a single transmission matrix or on the autocorrelation of transmitted speckle patterns would fail. The simple system of two diffusers excludes the possibility of the ME to influence image reconstruction, which we verified by projecting a simple three-dot pattern shown in Fig. 1(b) and calculating the autocorrelation $C(\Delta r) = \langle \int I(r) I(r+\Delta r) / \int I^2(r) \rangle$ of the scattered light far-field speckle patterns I (obtained by removing the imaging system), averaged over 600 different diffuser realizations. As we can see in the middle panel of Fig. 1(b), the autocorrelation of the light scattered by a single diffuser shows a clear hexagonal pattern (the autocorrelation of the projected pattern), indicating the presence of linear correlations and ME. The right panel shows the same autocorrelation for the two spatially separated diffusers characterized by the absence of any structure, indicating the absence of any ME.

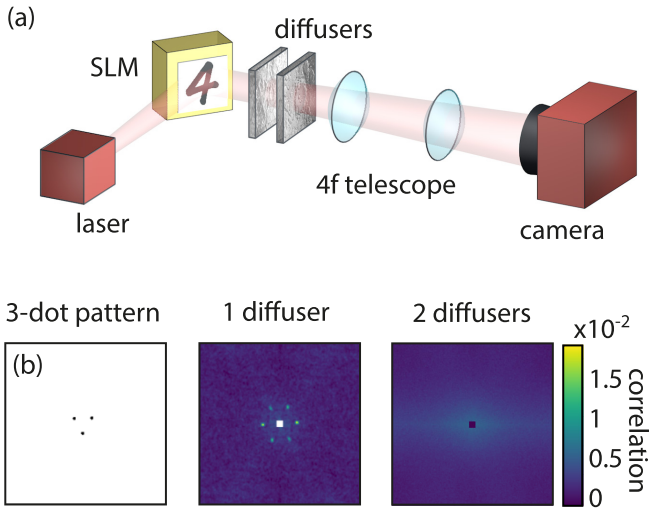

FIG. 1. Experimental setup and memory effect. (a) Experimental setup: A laser illuminates a SLM (DMD or liquid crystal) which is imaged onto the camera (CCD). The scattering medium is made from one or two glass diffusers separated by 5 mm. (b) A three-dot pattern projected by the DMD was used to test for the presence of the memory effect (the separation between the dots was 0.8 mm). With one diffuser, the averaged output speckle autocorrelation clearly shows correlation features, indicating the presence of the ME. With two diffusers, the correlation pattern completely disappears, indicating the absence of any ME. Central peak with $C = 1$ is removed for better visibility.

III. STATISTICAL DEPENDENCIES IN SCATTERED LIGHT

To track the statistical dependencies between the input and output light intensities for such a system one can build a probability density function (PDF) $P[I(\mathbf{r}_{\text{in}}), I(\mathbf{r}_{\text{out}})]$, where $I(\mathbf{r}_{\text{in}})$ and $I(\mathbf{r}_{\text{out}})$ are the input and output light intensities, respectively. This is a very complicated object since it captures all the possible combinations of the input and output (continuous) intensities at arbitrary positions in front and behind the scatterer. Assuming the intensity is discretized at N_i levels and there are N_{in} and N_{out} observation points in the input and output, respectively, the total dimension of this PDF would be $N_i^{N_{\text{in}}} \times N_i^{N_{\text{out}}}$. We numerically study a low-dimensional version of this distribution with $N_i = 2$ and $N_{\text{in}} = N_{\text{out}} = 9$ to get an estimate of the lower bound of the mutual information (MI) between the input and output light distributions.

We modeled the scattering layers by applying a random phase mask to the input field and calculating the output pattern at a particular distance from the incident plane using the standard Fresnel propagation formula (see Supplemental Material [30] for more model details). The spatial profiles that we use as the phase masks have two characteristic parameters: average width of the features (autocorrelation width) and their average height (standard deviation of the profile). These two parameters determine the strength of the scattering. The input pattern was a set of nine Gaussian spots, each of their

amplitudes being an independent Bernoulli process. The input field therefore carries exactly nine bits of spatial information. We calculated the output patterns for each of the 512 combinations of the input spots, each for 1000 different realizations of the random phase masks. We then thresholded the resulting output patterns with respect to the average intensity, selected nine subregions of those binarized patterns and assigned numeric labels to each of the 512 possible combinations of zero or unit intensity within them. The histograms of the pattern labels over the disorder realizations can be interpreted as the conditional distributions of a joint PDF, given a particular input pattern. As all the input patterns are equiprobable, the joint PDF was obtained by simply stacking the conditional PDFs. The MI was then calculated using the standard formula

$$\mathcal{I} = H[P(I^{\text{inp}})] - H[P(I^{\text{inp}}|I^{\text{out}})]. \quad (1)$$

The first term is the entropy of the input intensity probability distribution (equal to nine bits) and the second term is the conditional entropy $H[P(I^{\text{inp}}|I^{\text{out}})] = \sum_i p_i H[P(I^{\text{inp}}|I^{\text{out}} = I_i^{\text{out}})]$, where p_i are the probabilities of different output patterns, $H[P(I^{\text{inp}}|I^{\text{out}} = I_i^{\text{out}})]$ are the conditional distributions given a particular output pattern outcome, and H is the standard entropy $H[P(x)] = -\sum_i P(x_i)\log_2[P(x_i)]$. To remove the bias of the conditional entropy estimator, we use its jackknife version [31] (see Supplemental Material [30] for more details).

Figure 2(a) shows example input and simulated output patterns for two different bilayer phase mask realizations: in the left panel the roughness height standard deviation of the phase masks was 1.3 μm, while in the right one it was 13 μm. The broader intensity distribution in the second case reflects the stronger scattering conditions. The resulting simulated PDFs, shown in Fig. 2(b) indicate that in the stronger scattering scenario (right panel) the resulting PDF is closer to a simple product of the conditional distributions: some output patterns are more probable than the others, but the conditional distributions given a particular input do not differ significantly. In the weaker scattering case (left panel) the conditional distributions show much more variation, thus one would expect more MI in this case. Indeed the amount of MI versus the separation, d_o, of pixels in the nine spot output pattern is shown in Fig. 2(c) and indicates that there is always more information in the weak scattering case (left panel) compared to the stronger scattering case (right panel). These graphs also show that the information is not uniformly spread across the speckle image for weaker scattering: more information is contained at a distance of around 100 μm from the center, where the output speckle varies more versus dynamic disorder. The uniform value of the MI in the strong scattering case indicates that the speckles now vary uniformly across the camera image plane when the disorder is changed.

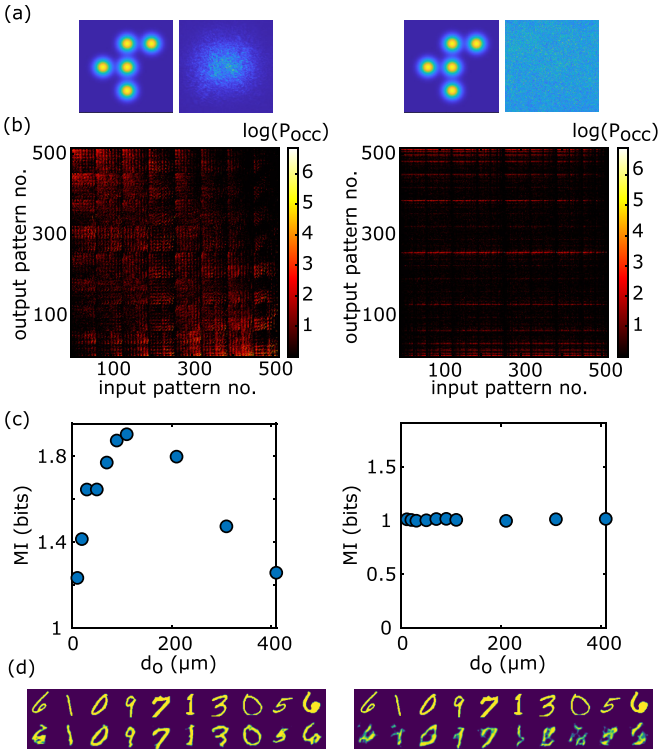

FIG. 2. Numerical simulations and mutual information between input and output intensity patterns. Left column corresponds to the phase masks with a height standard deviation of 1.3 μm, right column to 13 μm. (a) Examples of the input and output simulated patterns used for MI estimation. FWHM of the input spots is 20 μm. The separation between their centers is 40 μm. The speckle images have 1×1 mm field of view. (b) Joint PDFs showing the number of occurrences of a particular input and output pattern pair. (c) MI in bits calculated from the PDFs. d_o is the separation of the pixels in the output pattern see Supplemental Material [30] for the exact model description. (d) Examples of the image reconstruction through an unseen phase-mask realization: Top row shows the input images, the lower row shows the reconstructed images. The reconstruction MSE is 0.059 and 0.078 for the left and right panels, respectively.

IV. IMAGING THROUGH SCATTERING MEDIA BEYOND THE MEMORY EFFECT

The presence of MI, however, does not of course guarantee the existence of an easy procedure for its recovery. We show that these statistical dependencies can be picked up by an ANN that is trained to transform output speckle patterns into (unseen) input images of objects placed before the scatterer. We first verified this on our numerical model. We calculated the speckle patterns in the bilayer phase mask simulation with the first 1000 MNIST digit images being the input and changing the disorder for each consecutive input image. We repeated this process 32 times using an independent set of phase-masks each time to form a dataset of 32 000 speckle/digit-image pairs, which was then used to train a U-net ANN. The imaging performance was tested on a separate set of speckle-image pairs, where neither the input images nor the disorder realization has been used in a training dataset. Examples of the testing results are shown in Fig. 2(d). The left panel for the weaker scattering case clearly shows the ability to recover unseen images even in the absence of any linear correlations. As one might expect from Fig. 2(c), the stronger scattering case that has a lower MI, also shows worse image reconstruction although, even with just one bit of MI, the main features are still recognizable. We also experimentally verified these findings. We measured the output speckle patterns corresponding to 1000 MNIST digit input images [32], with a

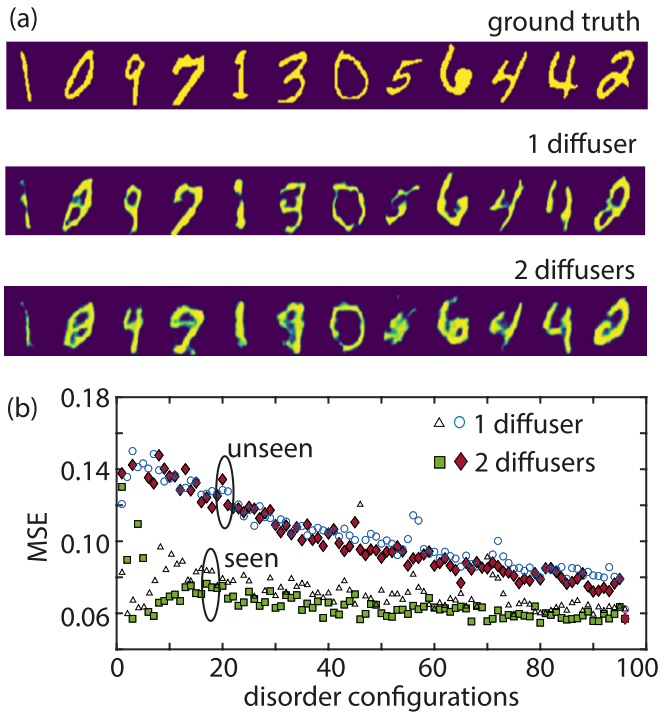

FIG. 3. Image reconstruction results. (a) Examples of ground truth images (unseen during ANN training) together with image reconstructions (after training on 95 different disorder configurations) with one diffuser and two diffusers. (b) Reconstruction mean-squared error (MSE) for increasing number of disorder configurations used for training, showing how MSE improves continuously with increasing number of training configurations for unseen images.

digital mirror device (DMD) used as an SLM and repeated this by translating the scattering medium in the transverse plane for 96 different nonoverlapping regions. Therefore, each of the 96 repetitions involves completely different microscopic realizations of the random medium, albeit with the same average property, i.e., grit. This data are used to train a U-net ANN [27], following the same architecture explained in detail in Ref. [28].

Examples of ANN image reconstruction of digits (unseen during the training) are shown in Fig. 3(a). The top row shows ground truth examples with the reconstruction with just one diffuser (middle row) and then for two diffusers (lower row) from which it can be seen that despite the absence of ME, the ANN is still able to reconstruct hidden images successfully. As shown in Fig. 3(b) the reconstruction mean squared error continues to decrease with the number of disorder configurations used for training. Moreover, the MSE for both one and two diffusers decreases at a similar rate and with the same absolute values. This indicates that the ME is never actually playing a major role in the ANN reconstruction, regardless of its presence. This is rather surprising as one might expect a strong linear correlation property to be the dominant feature captured by the high-dimensional interpolation properties of ANNs. Rather, our findings indicate that the ANN is extracting information from the nonlinear dependency and possibly not only here, but also in previous studies that relied on simple single-scattering systems [27,33].

V. CONCLUSION

We showed the presence of statistical dependencies beyond linear correlations within the optical scattered intensities by calculating the MI of an input-output probability distribution for a system where no linear correlations are possible. Recent work also showed how these ANN approaches can be extended to imaging through not only dynamic random media, but also at different depths and defocus conditions, thus indicating that these results are not specific to a given imaging system [29,33].

Looking forward, a first obvious extension would be to apply these results to imaging through inherently dynamical and changing scattering media such as living tissue or fog. This leads to further questions, such as how these results extend to the case in which one physically modifies the microscopic properties, e.g., average scatterer size rather than moving a diffuser that has fixed statistical properties. There are also implications for applications of scattering media for secure encoding and transmission of information. These systems typically rely on the fact that any given random medium is practically unclonable and therefore acts as one-pad encryption key. However, our results seem to imply that knowledge of the statistical properties of the scattering medium (e.g., the average distribution of refractive index perturbations) is sufficient to decode scrambled information, with important implications on the security of these encoding approaches [34,35]. Finally, identification of the shape of the nonlinear correlations could provide insight for their in-depth theoretical study in analogy to the theory of linear correlations [2,3].

All the data and codes related to this work are available at Ref. [36].

ACKNOWLEDGMENTS

We acknowledge discussions with J. Bertolotti. This work was supported by the Royal Academy of Engineering, Chair in Emerging Technologies scheme, by the Engineering and Physical Sciences Research Council of the UK (EPSRC) Grants No. EP/T00097X/1 and No. EP/S026444/1 and by the UK MOD University Defence Research Collaboration (UDRC) in Signal Processing.

[1] J. Goodman, *Speckle Phenomena in Optics: Theory and Applications* (Roberts & Co, Englewood, CO, 2007).

[2] R. Berkovits and S. Feng, Correlations in coherent multiple scattering, Phys. Rep. **238**, 135 (1994).

[3] S. Feng, C. Kane, P. A. Lee, and A. D. Stone, Correlations and Fluctuations of Coherent Wave Transmission through Disordered Media, Phys. Rev. Lett. **61**, 834 (1988).

[4] I. Freund, M. Rosenbluh, and S. Feng, Memory Effects in Propagation of Optical Waves through Disordered Media, Phys. Rev. Lett. **61**, 2328 (1988).

[5] I. Freund, Looking through walls and around corners, Physica A **168**, 49 (1990).

[6] J. Bertolotti, E. G. van Putten, C. Blum, A. Lagendijk, W. L. Vos, and A. P. Mosk, Non-invasive imaging through opaque scattering layers, Nature (London) **491**, 232 (2012).

[7] O. Katz, P. Heidmann, M. Fink, and S. Gigan, Non-invasive single-shot imaging through scattering layers and around corners via speckle correlations, Nat. Photon. **8**, 784 (2014).

[8] I. Starshynov, A. M. Paniagua-Diaz, N. Fayard, A. Goetschy, R. Pierrat, R. Carminati, and J. Bertolotti, Non-Gaussian Correlations between Reflected and Transmitted Intensity Patterns Emerging from Opaque Disordered Media, Phys. Rev. X **8**, 021041 (2018).

[9] A. M. Paniagua-Diaz, I. Starshynov, N. Fayard, A. Goetschy, R. Pierrat, R. Carminati, and J. Bertolotti, Blind ghost imaging, Optica **6**, 460 (2019).

[10] T. W. Anderson, *An Introduction to Multivariate Statistical Analysis* (Wiley-Interscience, Hoboken, NJ, 2003).

[11] G. J. Foschini and M. J. Gans, On limits of wireless communications in a fading environment when using multiple antennas, Wireless Pers. Commun. **6**, 311 (1998).

[12] A. L. Moustakas, H. U. Baranger, L. Balents, A. M. Sengupta, and S. H. Simon, Communication through a diffusive medium: Coherence and capacity, Science **287**, 287 (2000).

[13] S. H. Simon, A. L. Moustakas, M. Stoytchev, and H. Safar, Communication in a disordered world, Phys. Today **54**, 38 (2001).

[14] J. Stäring, A. Eriksson, and B. Mehlig, Fluctuations of the shannon capacity in a rayleigh model of wireless communication, Physica Status Ssolidi (b) **241**, 2136 (2004).

[15] N. Byrnes and M. R. Foreman, Universal bounds for imaging in scattering media, New J. Phys. **22**, 083023 (2020).

[16] C. W. Beenakker, Random-matrix theory of quantum transport, Rev. Mod. Phys. **69**, 731 (1997).

[17] S. M. Popoff, G. Lerosey, R. Carminati, M. Fink, A. C. Boccara, and S. Gigan, Measuring the Transmission Matrix in Optics: An Approach to the Study and Control of Light Propagation in Disordered Media, Phys. Rev. Lett. **104**, 100601 (2010).

[18] E. G. van Putten and A. P. Mosk, The information age in optics: Measuring the transmission matrix, Physics **3**, 22 (2010).

[19] S. Popoff, G. Lerosey, M. Fink, A. C. Boccara, and S. Gigan, Image transmission through an opaque material, Nat. Commun. **1**, 81 (2010).

[20] M. Plöschner, T. Tyc, and T. Čižmár, Seeing through chaos in multimode fibres, Nat. Photon. **9**, 529 (2015).

[21] A. Albertazzi, Jr., M. Viotti, F. Silva, C. Veiga, E. Barrera, M. Benedet, A. Fantin, and D. Willemann, Speckle interferometry in harsh environments: Design considerations and successful examples, in *Optical Micro-and Nanometrology VII* (SPIE, Bellingham, WA, 2018), Vol. 10678, p. 1067802.

[22] T. Ando, R. Horisaki, and J. Tanida, Speckle-learning-based object recognition through scattering media, Opt. Express **23**, 33902 (2015).

[23] G. Satat, M. Tancik, O. Gupta, B. Heshmat, and R. Raskar, Object classification through scattering media with deep learning on time resolved measurement, Opt. Express **25**, 17466 (2017).

[24] A. Turpin, I. Vishniakou, and J. Seelig, Light scattering control in transmission and reflection with neural networks, Opt. Express **26**, 30911 (2018).

[25] S. Li, M. Deng, J. Lee, A. Sinha, and G. Barbastathis, Imaging through glass diffusers using densely connected convolutional networks, Optica **5**, 803 (2018).

[26] G. Barbastathis, A. Ozcan, and G. Situ, On the use of deep learning for computational imaging, Optica **6**, 921 (2019).

[27] O. Ronneberger, P. Fischer, and T. Brox, U-net: Convolutional networks for biomedical image segmentation, in *Medical Image Computing and Computer-Assisted Intervention – MICCAI 2015*, edited by N. Navab, J. Hornegger, W. M. Wells, and A. F. Frangi (Springer International Publishing, Cham, Switzerland, 2015), pp. 234–241.

[28] Y. Li, Y. Xue, and L. Tian, Deep speckle correlation: A deep learning approach toward scalable imaging through scattering media, Optica **5**, 1181 (2018).

[29] S. Resisi, S. M. Popoff, and Y. Bromberg, Image transmission through a dynamically perturbed multimode fiber by deep learning, Laser Photon. Rev. **15**, 2000553 (2021).

[30] See Supplemental Material at http://link.aps.org/supplemental/10.1103/PhysRevResearch.4.L022033 for additional details on the numerical model and mutual information calculations..

[31] L. Paninski, Estimation of entropy and mutual information, Neural Comput. **15**, 1191 (2003).

[32] MNIST image database: http://yann.lecun.com/exdb/mnist/.

[33] Y. Li, S. Cheng, Y. Xue, and L. Tian, Displacement-agnostic coherent imaging through scatter with an interpretable deep neural network, Opt. Express **29**, 2244 (2021).

[34] R. Uppu, T. A. Wolterink, S. A. Goorden, B. Chen, B. Škorić, A. P. Mosk, and P. W. Pinkse, Asymmetric cryptography with physical unclonable keys, Quantum Sci. Technol. **4**, 045011 (2019).

[35] A. Fratalocchi, A. Fleming, C. Conti, and A. D. Falco, NIST-certified secure key generation via deep learning of physical unclonable functions in silica aerogels, Nanophotonics **10**, 20200368 (2020).

[36] Dataset for the paper Statistical Dependencies Beyond Linear Correlations in Light Scattered by Disordered Media, http://doi.org/10.5525/gla.researchdata.1089.